





# Polydopamine Modified Ceria Nanorods Alleviate Inflammation in Colitis by Scavenging ROS and Regulating Macrophage M2 Polarization

Bingqing Zhang , Qiang Li , Qinglin Xu, Baochao Li , Heng Dong , Yongbin Mou

Nanjing Stomatological Hospital, Affiliated Hospital of Medical School, Nanjing University, Nanjing, People's Republic of China

\*These authors contributed equally to this work

Correspondence: Yongbin Mou; Heng Dong, Nanjing Stomatological Hospital, Medical School of Nanjing University, #30 Zhongyang Road, Nanjing, 210008, People's Republic of China, Email [yongbinmou@nju.edu.cn](mailto:yongbinmou@nju.edu.cn); [dongheng90@smail.nju.edu.cn](mailto:dongheng90@smail.nju.edu.cn)

**Background:** Inflammatory bowel disease (IBD) is closely related to higher intracellular oxidative stress. Therefore, developing a novel method to scavenge the harmful reactive oxygen species (ROS) and alleviate colon inflammation to treat IBD is a promising strategy.

**Methods:** CeO<sub>2</sub>@PDA-PEG (CeO<sub>2</sub>@PP) were synthesized by modifying ceria (CeO<sub>2</sub>) nanorods with polydopamine (PDA) and polyethylene glycol (PEG). The ROS scavenging ability of CeO<sub>2</sub>@PP was detected by using flow cytometry and confocal laser scanning microscope (CLSM). The anti-inflammatory ability of CeO<sub>2</sub>@PP was determined in vitro by treating lipopolysaccharide (LPS)-stimulated RAW 264.7 macrophages. The biocompatibility of CeO<sub>2</sub>@PP was evaluated in vivo and in vitro. Moreover, the therapeutic effects of CeO<sub>2</sub>@PP in vivo were estimated in a dextran sulfate sodium salt (DSS)-induced colitis mouse model.

**Results:** Physicochemical property results demonstrated that PDA and PEG modification endowed CeO<sub>2</sub> nanorods with excellent dispersibility and colloidal stability. CeO<sub>2</sub>@PP maintained superior enzyme-like activity, including superoxide dismutase (SOD) and catalase (CAT), indicating antioxidant ability. Moreover, in vitro results showed that CeO<sub>2</sub>@PP with PDA promotes LPS-induced RAW 264.7 macrophages into M2-type polarization. In addition, in vitro and in vivo results showed that CeO<sub>2</sub>@PP have great biocompatibility and biosafety. Animal experiments have shown that CeO<sub>2</sub>@PP have excellent anti-inflammatory effects against DSS-induced colitis and effectively alleviated intestinal mucosal injury.

**Conclusion:** The nanoplatform CeO<sub>2</sub>@PP possessed excellent antioxidant and anti-inflammatory properties for scavenging ROS and modulating macrophage polarization, which is beneficial for efficient colitis therapy.

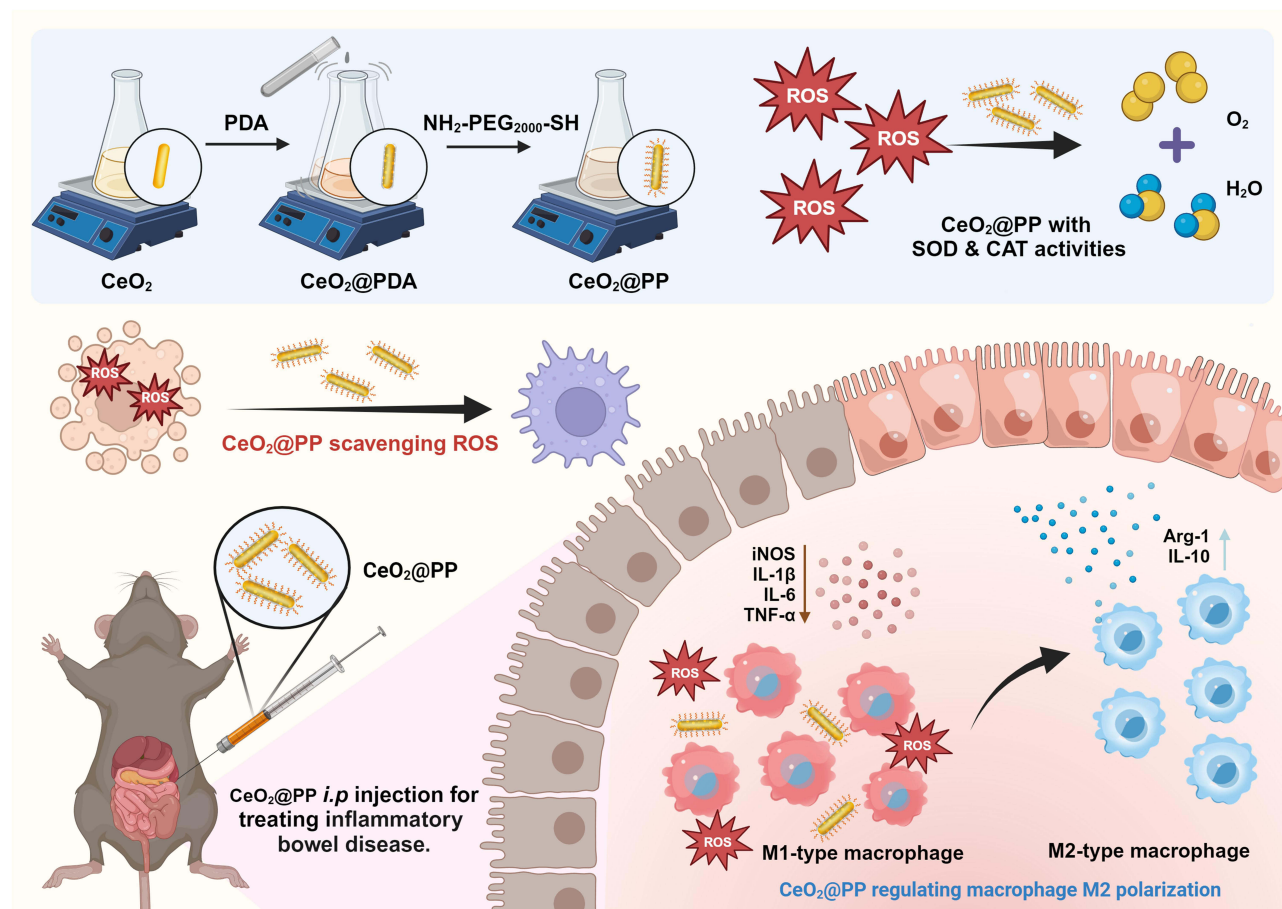
**Keywords:** ceria, PDA, nanozyme, antioxidation, anti-inflammation, macrophage polarization, colitis

## Introduction

Inflammatory bowel disease (IBD), including ulcerative colitis and Crohn's disease, is a group of diseases that can cause recurrent chronic inflammation of the gastrointestinal tract.<sup>1</sup> The prevalence of IBD is increasing every year.<sup>2</sup> More seriously, multiple scholars have found that IBD patients have a significantly increased risk of colorectal cancer due to recurrent lesions in the lining of the colon and rectum.<sup>3</sup> It is widely believed that the excessive production of reactive oxygen species (ROS) in the colon is one of the key factors aggravating IBD.<sup>4</sup> When excessive ROS cannot be removed in time, the oxidative stress of mucosal cells will significantly enhance the permeability of the intestinal membrane and initiate a cascade of destructive immune responses in the intestine, eventually causing intestinal mucosa damage.<sup>5</sup> The damage and inflammatory response of the colon and rectum will break down its antioxidant defense mechanism, make the intestinal mucosa more susceptible to ROS stimulation, and further aggravate IBD.<sup>6</sup>

Currently, there is still no ideal treatment for IBD.<sup>7</sup> The clinical treatment for patients with moderate IBD is to modify the diet structure to eliminate persistent irritants and to use antibiotics or immunosuppressants to relieve inflammation.

## Graphical Abstract



For patients with severe IBD, surgical removal of the damaged part of the intestine is needed to control the progression of IBD. However, these treatments are not only dissatisfactory but also produce significant side effects.<sup>8,9</sup> Given the important role of oxidative stress in the pathological process of IBD, antioxidant therapy has been used in many experiments for the treatment of IBD and has made significant progress.<sup>10</sup> These natural or synthetic antioxidants are well tolerated and have minimal side effects.<sup>11</sup> Therefore, it may be a promising direction for future research. There are many kinds of ROS scavengers, and how to find suitable anti-ROS drugs for IBD treatment is the current focus.

Some naturally occurring enzymes such as superoxide dismutase (SOD) and catalase (CAT) can reduce intracellular ROS content.<sup>12,13</sup> However, these natural enzymes are easily degraded and difficult to prepare and store, limiting their direct application in clinical work.<sup>14</sup> In addition, many natural enzymes are catalytically active against only a single species of oxygen radical. To overcome these challenges, artificial nanozymes have been developed for scavenging ROS due to their many advantages.<sup>15</sup> Nanozymes with ceria (CeO<sub>2</sub>) as the main component have received extensive attention in recent years due to their SOD and CAT activities, which can be used to scavenge ROS and thereby protect cells.<sup>16</sup> The Ce ion in CeO<sub>2</sub> crystal has both tetravalent (Ce<sup>4+</sup>) and trivalent (Ce<sup>3+</sup>) oxidation states, in which Ce<sup>4+</sup> can oxidize H<sub>2</sub>O<sub>2</sub> through CAT activity, and Ce<sup>3+</sup> is responsible for scavenging O<sub>2</sub><sup>•-</sup> by the SOD characteristics.<sup>17</sup> The coexistence and transition between Ce<sup>4+</sup> and Ce<sup>3+</sup> impart a sustained catalytic effect of CeO<sub>2</sub>.<sup>18</sup> Therefore, ceria-related nanozymes have been investigated as antioxidants for the treatment of ROS-associated diseases, such as atherosclerosis, rheumatoid arthritis and hepatitis.<sup>17</sup> However, traditional CeO<sub>2</sub>-based nanomaterials are prone to aggregation and sedimentation in solution, which is not only unfavorable for external studies, but also leads to internal safety problems.<sup>19</sup> A common

solution is to modify CeO<sub>2</sub> with a biocompatible coating on the surface to improve its dispersion and stability in aqueous solution.<sup>18</sup>

Understanding the role of macrophages in the pathogenesis of IBD is also important. Intestinal macrophages can be categorized into two distinct subsets, including pro-inflammatory (M1) and anti-inflammatory (M2) macrophages.<sup>20</sup> M1 macrophages induce high levels of proinflammatory cytokines, combined with high levels of ROS, resulting in disruption of the intestinal epithelial barrier. Compared to M1 macrophages, M2 macrophages can stimulate angiogenesis and initiate repair and functional recovery of the intestinal epithelial barrier. Polydopamine (PDA) has satisfactory biodegradability and biocompatibility because of its similar structure to melanin.<sup>21</sup> Previous studies have shown that PDA can greatly reduce the inflammatory response, scavenge ROS in inflammatory tissues and direct macrophage polarization toward the M2 phenotype.<sup>22</sup> Moreover, the molecular structure of PDA contains many functional groups such as amine groups and catechols, which allows further chemical modification of this nanomaterial.<sup>23,24</sup> For example, when polyethylene glycol (PEG) is coupled to the PDA coating via the Michael addition reaction and Schiff base reaction,<sup>25</sup> the nanomaterials will be more easily bound to the cell membrane and taken up by the cells.

It has been reported that modification of CeO<sub>2</sub> nanomaterials with PEG can improve their dispersibility and stability due to the steric hindrance effect of the polymer.<sup>26</sup> In addition, there are many physical forms of CeO<sub>2</sub>, among which CeO<sub>2</sub> nanorods (CeO<sub>2</sub> NRs) have a larger surface area and looser packing than ordinary particles, and most importantly, they have higher catalytic performance.<sup>27</sup> Herein, we synthesized CeO<sub>2</sub>@PDA-PEG (CeO<sub>2</sub>@PP) by modifying CeO<sub>2</sub> NRs with a PDA coating and PEG conjugation for colitis treatment. CeO<sub>2</sub>@PP exhibits excellent stability and biocompatibility and can serve as an artificial nanozyme with SOD and CAT activities to scavenge cellular ROS. Moreover, CeO<sub>2</sub>@PP can also regulate macrophage polarization from the M1 to M2 phenotype and resume immune homeostasis to relieve colitis. This work provides a novel strategy that applies CeO<sub>2</sub>@PP as a potential therapeutic agent for treating colitis by scavenging intracellular ROS and regulating macrophage polarization.

## Materials and Methods

### Materials in Synthesis

CeO<sub>2</sub> NRs (XF135) were obtained from Jiangsu XFNano Materials Tech. Co. Ltd. Dopamine hydrochloride was purchased from Sigma (Sigma-Aldrich, USA) and Thiol-PEG<sub>2000</sub>-Amine (NH<sub>2</sub>-PEG<sub>2000</sub>-SH) was purchased from Solarbio (China). Tris and concentrated hydrochloric acid (HCl, 36–38 wt%) were purchased from Sinopharm Chemical Reagent Co. Ltd. (Shanghai, China). Ethyl-carbodiimide hydrochloride (EDC), N-hydroxy succinimide (NHS) and cyanine 5.5 (Cy5.5) amine dye were purchased from Yien Chemical Technology Co. Ltd. (Shanghai, China). Deionized water was obtained by a Milli-Q water purification system with a resistivity of 18 MΩ·cm (Millipore, USA).

### Synthesis of CeO<sub>2</sub>@PP

The procedure of modifying the PDA membrane to the surface of CeO<sub>2</sub> NRs was performed as previously reported.<sup>28</sup> Briefly, 10 mg of CeO<sub>2</sub> NRs was mixed into 10 mL of Tris hydrochloride (Tris-HCl) buffer (pH 8.5, 10 mM), and the mixture was sonicated for 30 min to evenly disperse the nanorods. After that, 20 mg dopamine hydrochloride was mixed into the system with continuous stirring at room temperature, and the polymerization reaction fully occurred by ultrasonic shaking for 3 h. The supernatant after the reaction was removed by centrifugation at 12,000 rpm for 30 min and then we recovered the precipitate. The non-reactive dopamine oligomers and dopamine molecules were removed by washing with ultrapure water. Finally, PDA-coated CeO<sub>2</sub> (CeO<sub>2</sub>@PDA) were collected. We next stabilized CeO<sub>2</sub>@PDA with an outer layer of NH<sub>2</sub>-PEG<sub>2000</sub>-SH on the PDA shell via Michael addition and Schiff base reactions.<sup>25</sup> The specific synthesis process is simply mixing CeO<sub>2</sub>@PDA with NH<sub>2</sub>-PEG<sub>2000</sub>-SH at a mass ratio of 1: 4 under magnetic stirring at 4 °C for 12 h. After washing three times with ultrapure water and centrifugation, the products of CeO<sub>2</sub>@PDA-PEG (CeO<sub>2</sub>@PP) were collected for further characterization and experiments.

## Physicochemical Properties of CeO<sub>2</sub>@PP

We observed the morphology and structure of CeO<sub>2</sub> NRs and CeO<sub>2</sub>@PP using transmission electron microscope (TEM, Talos™ F200X G2 TEM). The element mapping images of CeO<sub>2</sub>@PP were taken by high resolution transmission electron microscope (HRTEM, FEI Talos F200S). By using dynamic light scattering (DLS, Malvern Zetasizer Nano ZS90), we examined the hydrodynamic size, size distribution range and the zeta potential of CeO<sub>2</sub> NRs and CeO<sub>2</sub>@PP. Homogeneous CeO<sub>2</sub> NRs and CeO<sub>2</sub>@PP solutions (1 mg/mL) were prepared in H<sub>2</sub>O, PBS and DMEM, and then colloidal stability was evaluated after standing for 24 h. X-ray photoelectron spectroscopy (XPS, Thermo Scientific K-Alpha) analysis was performed to determine the surface valence of Ce<sup>3+</sup> and Ce<sup>4+</sup>. Fourier transform infrared spectroscopy (FT-IR, Thermo Scientific Nicolet iS20) was used to measure changes in the chemical structure of CeO<sub>2</sub> following functionalization with PDA and PEG. The SOD-like activities of CeO<sub>2</sub> NRs and CeO<sub>2</sub>@PP were measured by the Total SOD Assay Kit (Beyotime, China) according to the manufacturer's instructions. The CAT-like activities of CeO<sub>2</sub> NRs and CeO<sub>2</sub>@PP were measured by the Catalase Assay Kit (Beyotime, China) according to the manufacturer's instructions. CeO<sub>2</sub> NRs and CeO<sub>2</sub>@PP (20 µg/mL) were added to an aqueous solution containing the same concentration of H<sub>2</sub>O<sub>2</sub> to further test the CAT-like activity, and the dissolved O<sub>2</sub> was tested using a JPSJ-605F dissolved oxygen instrument (INESA Scientific Instrument, China).

## Biocompatibility of CeO<sub>2</sub>@PP in vitro

RAW 264.7 macrophages were obtained from the Cell Bank of the Chinese Academy of Sciences (Shanghai, China). RAW 264.7 cells were cultured using complete DMEM (Gibco, USA) containing 1% penicillin–streptomycin (Gibco) and 10% fetal bovine serum (FBS, Gibco) in an incubator with an environment stabilized at 37 °C. To determine the biosafety of CeO<sub>2</sub>@PP, RAW 264.7 cells were plated in 96-well plates (1×10<sup>4</sup> cells/well). After the cells adhered completely, gradient concentrations of CeO<sub>2</sub>@PP (0, 20, 40, and 80 µg/mL) were added to the wells of plates for 24 h, and each concentration was detected in 3 duplicates. Cell viability was detected by the CCK-8 (Vazyme, China) method according to the manufacturer's instructions.

## Cell Uptake of CeO<sub>2</sub>@PP in vitro

Afterwards, Cy5.5 was covalently conjugated to CeO<sub>2</sub>@PP with the aid of EDC and NHS to test the cell uptake ability of CeO<sub>2</sub>@PP. One milligram of EDC, 1 mg of NHS and 500 µg of Cy5.5 were mixed in 5 mL of water and stirred for 3 h. Then 5 mg CeO<sub>2</sub>@PP was added to the mixture and stirred overnight. The products of CeO<sub>2</sub>@PP-Cy5.5 were collected after washing three times with ultrapure water and centrifugation. RAW 264.7 cells were plated in 12-well plates at a concentration of 1×10<sup>5</sup> cells/well and incubated for 12 h to allow cell adherence. CeO<sub>2</sub>@PP-Cy5.5 (20 µg/mL) was added to the plates and treated cells for 1 h, 3 h and 6 h, and each timepoint was duplicated for 3 wells. After three washes with PBS, the cells were collected, and the mean fluorescence intensity (MFI) of Cy5.5 was detected by flow cytometry.

## Protective Effect of CeO<sub>2</sub>@PP Against H<sub>2</sub>O<sub>2</sub>-Induced Cell Apoptosis in vitro

RAW 264.7 cells were seeded in 12-well culture plates at a concentration of 1×10<sup>5</sup> cells/well and incubated for 12 h to allow cell adherence. The cells were pretreated with CeO<sub>2</sub>@PP (20 µg/mL) dispersion for 12 h and then stimulated with H<sub>2</sub>O<sub>2</sub> (200 µM) for 12 h. An Annexin V-FITC/PI apoptosis detection kit (Vazyme, China) was used to analyze cell apoptosis. Briefly, after the adherent cells were blown down slightly and washed thoroughly, all cells were stained with 5 µL Annexin V-FITC and 5 µL propidium iodide (PI) at room temperature in the dark for 10 min. The proportion of apoptotic cells was detected by flow cytometry.

## Detection of the Intracellular ROS Scavenging Ability of CeO<sub>2</sub>@PP in vitro

CellROX Green (Thermo Fisher Scientific) was used to measure the level of intracellular superoxide. After entering the cell, CellROX Green generates green fluorescence, which is used to reflect the level of ROS. For flow cytometry, RAW 264.7 cells were grown in 24-well culture plates at 4×10<sup>4</sup> cells/well with CeO<sub>2</sub>@PP (20 µg/mL) for 12 h and then treated with LPS (200 ng/mL) for 12 h. After staining with CellROX Green in the dark for 30 min, the cells were collected by centrifugation and the fluorescence intensity was detected. For fluorescence image analysis, RAW 264.7 cells were grown in confocal dishes at 1×10<sup>5</sup> cells/mL with CeO<sub>2</sub>@PP (20 µg/mL) for 12 h, and then LPS (200 ng/mL) was added to



stimulate cells for 12 h except for the sham group. After staining with CellROX Green in the dark for 30 min, the cells were imaged by confocal laser scanning microscope (CLSM).

## Anti-Inflammatory Activities of CeO<sub>2</sub>@PP in vitro

To investigate the anti-inflammatory polarization efficacy of CeO<sub>2</sub>@PP on macrophages, LPS (200 ng/mL)-stimulated RAW 264.7 cells were used as the inflammatory model to evaluate the anti-inflammatory activities of CeO<sub>2</sub>@PP (20 µg/mL). We labeled M1 macrophages with anti-CD86 and labeled M2 macrophages with anti-CD206, and then analyzed macrophage phenotypic switching by flow cytometry. The medium of RAW 264.7 cells with different treatments was collected for the next assessment of IL-6 proinflammatory cytokines by a mouse IL-6 enzyme linked immunosorbent assay (ELISA) kit (Multisciences, China) according to the manufacturer's instructions.

In addition, the expression of inflammatory mRNA in the RAW 264.7 inflammatory model was detected by RT-qPCR. Briefly, mRNA was extracted from RAW 264.7 cells using the *SteadyPure* Universal RNA Extraction Kit (Accurate Biology) and then converted to cDNA with RT Master Mix (Vazyme). The cDNA was analyzed by RealTime PCR using Taq Pro Universal SYBR qPCR Master Mix (Vazyme). The mRNA expression levels of M1 phenotype-related biomarkers, including inducible nitric oxide synthase (iNOS), interleukin 6 (IL-6), tumor necrosis factor alpha (TNF-α), and interleukin 1 beta (IL-1β), and M2 phenotype-related biomarkers, including arginase 1 (Arg-1) and interleukin 10 (IL-10), were calculated. The mRNA expression levels were calculated using the  $2^{-\Delta\Delta Ct}$  method, and all the resulting data were normalized to the housekeeping gene glyceraldehyde-3-phosphate dehydrogenase (GAPDH). Primer sequences for qPCR are shown in [Table S1](#).

## Hemolysis Assay of CeO<sub>2</sub>@PP

The erythrocytes were obtained by centrifuging the blood at 2000 rpm for 10 min. Erythrocytes were washed three times with PBS and finally diluted in 0.5 mL of PBS. For the hemolysis assay, 0.5 mL of different concentrations of CeO<sub>2</sub>@PP (5, 10, 20, 40 µg/mL) were added to the erythrocyte solution. The other two groups were treated with PBS (0.5 mL) as a negative control group and distilled water (0.5 mL) as a positive control group. After 3 h of incubation in a 37 °C water bath, the suspension was centrifuged at 1000 rpm for 5 min. The absorbance value (545 nm) of the supernatant was measured by a microplate reader. The hemolysis rate was calculated according to the following formula:<sup>29</sup>

$$\text{Hemolysis rate (\%)} = (\text{OD}_{\text{test}} - \text{OD}_{\text{nc}}) / (\text{OD}_{\text{pc}} - \text{OD}_{\text{nc}}) \times 100\%.$$

OD<sub>test</sub>, OD value of the sample; OD<sub>pc</sub>, OD value of the positive control; OD<sub>nc</sub>, OD value of the negative control.

## In vivo Toxicity Test of CeO<sub>2</sub>@PP

The toxicity of CeO<sub>2</sub>@PP to major organs was evaluated by histopathological observation. Specifically, healthy mice were intraperitoneally injected with PBS or CeO<sub>2</sub>@PP (20 µg) on days 2, 4, 6, and 8. At day 10, the heart, liver, spleen, lung, and kidney were collected for H&E staining and pathological observation. In addition, the following standard hematological markers in blood were assessed: white blood cells (WBC), red blood cell (RBC), hemoglobin (HGB), hematocrit (HCT), mean corpuscular volume (MCV), and mean corpuscular hemoglobin concentration (MCHC). The following blood biochemistry parameters were also examined: alanine transaminase (ALT), aspartate transaminase (AST), blood urea nitrogen (BUN), and creatinine (CRE).

## Animal Colitis Model Establishment and Treatment with CeO<sub>2</sub>@PP

Male C57BL/6 mice (6–8 weeks) were purchased from Shanghai Laboratory Animal Research Center (Shanghai, China). The animal experiments involved in this study were approved by the Animal Ethics and Welfare Committee of Nanjing University and all experimental procedures were performed in accordance with National Institutes of Health guidelines.

The colitis induced by dextran sulfate sodium salt (DSS, Aladdin Reagents, China) was chosen to evaluate the anti-inflammation of CeO<sub>2</sub>@PP in vivo. Specifically, 18 male C57BL/6 mice were randomly divided into three groups (n = 6) after one week of acclimation: (1) water + PBS *i.p.*, (2) 3% DSS + PBS *i.p.* and (3) 3% DSS + CeO<sub>2</sub>@PP *i.p.* The first group was given pure water to drink. The drinking water of group 2 and group 3 was replaced with an aqueous solution containing 3 wt% DSS and this day was designated as day 1. Mice group 3 were aseptically and intraperitoneally injected with CeO<sub>2</sub>@PP (20 µg) at day 2, 4, 6, and 8, while the mice in the first and second groups were injected with PBS at the

same time points. All mice were sacrificed on day 10. The entire colon of the mice was removed and the length of the colon was measured. Discarding 1 cm of the terminal colon tissue, 1 cm in length of the colon tissue was dissected for RNA extraction and the next 1 cm portion of the colon was placed in 4% paraformaldehyde (PFA) for subsequent histological testing. During the experimental period, we recorded each mouse's body weight and stool characteristics every other day. The disease activity index (DAI) was calculated according to previously reported criteria, which included the weight loss index, stool trait index and bloody stool index ([Table S2](#)).<sup>30</sup>

## In vivo Biodistribution of CeO<sub>2</sub>@PP

Male C57BL/6 mice (6 to 8 weeks) drank 3% DSS water for 7 days before the studies to generate the colitis model. Mice in the healthy group (n = 9) and DSS group (n = 9) were intraperitoneally injected with CeO<sub>2</sub>@PP-Cy5.5 (containing 100 µg/mL CeO<sub>2</sub>, 100 µL) and were euthanized and fluorescently imaged at 1.3 or 12 h post-injection. The major organs (heart, liver, spleen, lung, and kidney) and colon were collected and fluorescently imaged with in vivo imaging system (IVIS Lumina K Series III, Perkin Elmer).

## Pathological Evaluation

Colon tissue fixed in 4% paraformaldehyde was dehydrated, embedded in paraffin, and then cut into 5 µm thick histological sections. To visualize the morphology of colon tissue, sections were stained with hematoxylin and eosin (H&E) according to previously reported procedures.<sup>31</sup> The pathological images of dried sections were scanned and magnified using a slide scanner (3DHISTECH). The criteria for pathological scoring of colon tissue are shown in [Table S3](#).<sup>32</sup> IL-6 immunohistochemical staining was then performed on the colon tissue, and frozen sections of the colon were stained with DAPI and dihydroethidium (DHE, Sigma-Aldrich, USA) to test the ROS activity of colon tissues. Images were observed by confocal laser scanning microscope (CLSM).

## Flow Cytometry Assay of Peritoneal Macrophages in vivo

The murine peritoneal macrophages of mice in different treatment groups were harvested immediately after sacrifice, by washing the abdominal cavity with cold PBS. Cell suspensions were washed twice with cold DMEM as mentioned above, and then the cells were seeded and incubated for 3 h. The nonadherent cells were washed off with PBS, and then the isolated peritoneal cells were cultured in a 24-well plate at a concentration of  $2 \times 10^5$  cells/well for use. Macrophages were stained with anti-F4/80-Percp Cy5.5 and anti-CD86-PE antibodies for flow cytometry analysis.

## Mouse Colon Tissue RT-qPCR Analysis

To further verify the relative mRNA expression levels of key biomarkers in the colon samples, RT-qPCR was performed using distal colon tissue. The colon tissue was crushed in lysate by ultrasound, and after centrifugation, the supernatant was obtained. The next mRNA extraction, reverse transcription, amplification, assay and calculation steps followed the previously described steps. The relative mRNA expression levels of M1 phenotype-related biomarkers (iNOS, IL-6, TNF-α and IL-1β) were tested.

## Statistical Analysis

All analyses in the present study were performed with GraphPad Prism 8.0 software (CA, USA). The data are expressed as the mean ± standard deviation (S.D.). Unpaired two-tailed Student's t tests were used to determine the significant differences between two groups. Multiple comparisons were performed using one-way or two-way ANOVA, as appropriate. Differences with  $P < 0.05$  were considered statistically significant.

## Results

### Physicochemical Characterization of CeO<sub>2</sub>@PP

The synthesis procedure of CeO<sub>2</sub>@PP involved modifying CeO<sub>2</sub> NRs with PDA coating and PEG conjugation ([Figure 1A](#)). The morphology of the nanorods was obtained by TEM. As shown in [Figure 1B](#), characterization by TEM revealed CeO<sub>2</sub> NRs had an average length and diameter of  $18.49 \pm 0.71$  nm and  $5.30 \pm 0.22$  nm, respectively, as statistically obtained using ImageJ software

( $n = 16$ ). TEM of  $\text{CeO}_2\text{@PP}$  is shown in Figure 1C, and a thin layer ( $2.33 \pm 0.27$  nm) was observed after coating PDA and conjugating PEG on  $\text{CeO}_2$  NRs. The elemental mapping images on Figure 1D show that Ce, O, and N were homogeneously distributed in  $\text{CeO}_2\text{@PP}$ , which further confirmed the successful coating of PDA and PEG on the surface of  $\text{CeO}_2$ . The zeta potential of  $\text{CeO}_2$  NRs was  $-12.63 \pm 0.21$  mV, while it changed to  $-7.24 \pm 0.41$  mV after coating PDA and conjugating PEG on  $\text{CeO}_2$  NRs (Figure 1E). The hydrodynamic diameters were estimated using a DLS assay, and the diameters of  $\text{CeO}_2$  NRs ( $762.30 \pm 89.67$  nm) were approximately triple that of  $\text{CeO}_2\text{@PP}$  ( $206.20 \pm 3.67$  nm), indicating that the modification of  $\text{CeO}_2$  NRs can prevent nanoparticle aggregation in  $\text{H}_2\text{O}$  (Figure 1F). The stability of  $\text{CeO}_2$  and  $\text{CeO}_2\text{@PP}$  in  $\text{H}_2\text{O}$ , PBS and DMEM aqueous solutions was investigated after standing for 24 h. Noticeably, the pale yellow precipitates could be seen in the  $\text{CeO}_2$  solutions,

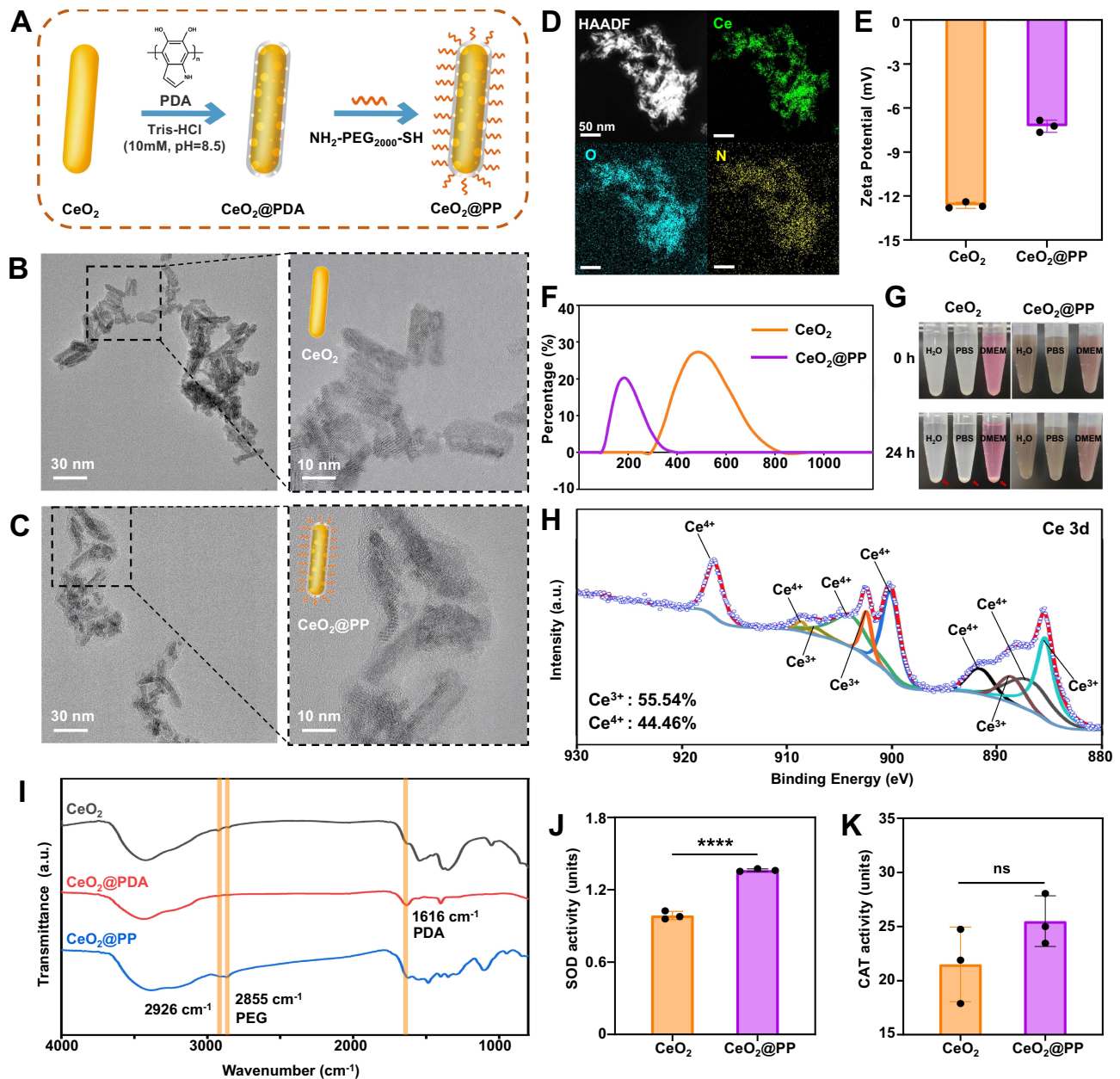


**Figure 1** Physicochemical characterization of  $\text{CeO}_2\text{@PP}$ . (A) Schematic illustration of the  $\text{CeO}_2\text{@PP}$  synthesis procedure. Transmission electron microscopic (TEM) images of (B)  $\text{CeO}_2$  NRs and (C)  $\text{CeO}_2\text{@PP}$ . (D) HRTEM and elemental mapping images of  $\text{CeO}_2\text{@PP}$ . (E) Zeta potential of  $\text{CeO}_2$  NRs and  $\text{CeO}_2\text{@PP}$  in  $\text{H}_2\text{O}$ . (F) DLS size distribution of  $\text{CeO}_2$  NRs and  $\text{CeO}_2\text{@PP}$ . (G) Representative images of  $\text{CeO}_2$  NRs and  $\text{CeO}_2\text{@PP}$  in different solutions ( $\text{H}_2\text{O}$ , PBS and DMEM culture medium). (H) Ce 3d XPS spectrum of  $\text{CeO}_2\text{@PP}$ . (I) FT-IR spectra of  $\text{CeO}_2$ ,  $\text{CeO}_2\text{@PDA}$  and  $\text{CeO}_2\text{@PP}$ . (J) SOD activity of  $\text{CeO}_2$  NRs and  $\text{CeO}_2\text{@PP}$ . (K) CAT activity of  $\text{CeO}_2$  NRs and  $\text{CeO}_2\text{@PP}$ . \*\*\*\* $P < 0.0001$ ; ns, not significant.



while there was no obvious precipitate in the  $\text{CeO}_2@\text{PP}$  solutions after 24 h of standing (Figure 1G). This suggests that PDA and PEG modification promote the colloidal stability of  $\text{CeO}_2$  NRs. The valence chemistry of  $\text{CeO}_2@\text{PP}$  was measured with XPS. As shown in Figure 1H, the XPS spectra of  $\text{CeO}_2@\text{PP}$  revealed that Ce existed in mixed valence states ( $\text{Ce}^{3+}$  and  $\text{Ce}^{4+}$ ). The six peaks at binding energies of 882.75 eV, 897.12 eV, 887.83 eV, 901.34 eV and 915.4 eV were identified as those of  $\text{Ce}^{4+}$ , while the peaks at 881.14 eV, 884.59 eV, 899.67 eV and 904.9 eV were assigned to  $\text{Ce}^{3+}$ .<sup>33</sup> By calculating the integral area of each peak, the ratio of  $\text{Ce}^{3+}$ :  $\text{Ce}^{4+}$  in  $\text{CeO}_2@\text{PP}$  was found to be 55.54%: 44.46%. The coating of PDA and PEG on  $\text{CeO}_2$  nanorods was further confirmed by Fourier transform infrared spectroscopy (FT-IR). As shown in Figure 1I, the IR absorption band near  $1616\text{ cm}^{-1}$  of  $\text{CeO}_2@\text{PDA}$  can be assigned to the C=C stretching vibration and N-H bending vibration from PDA, suggesting the successful coating of PDA on the surface of  $\text{CeO}_2$  NRs.<sup>34</sup> Furthermore, the IR absorption bands at  $2926\text{ cm}^{-1}$  and  $2855\text{ cm}^{-1}$  can be assigned to the C-H stretching vibrations from PEG, suggesting the successful coating of PEG on the surface of  $\text{CeO}_2@\text{PDA}$ .<sup>35</sup>

The SOD-like activity of different nanoparticles to scavenge  $\text{O}_2^{\cdot-}$  is shown in Figure 1J.  $\text{CeO}_2$  NRs and  $\text{CeO}_2@\text{PP}$  both showed SOD-like activity. The SOD activity of  $\text{CeO}_2@\text{PP}$  was obviously increased compared to the same concentration of  $\text{CeO}_2$ . Moreover, both  $\text{CeO}_2$  NRs and  $\text{CeO}_2@\text{PP}$  had considerable CAT-like activity to scavenge  $\text{H}_2\text{O}_2$  (Figure 1K). Although there was no significant difference in their CAT activities, the activity of  $\text{CeO}_2@\text{PP}$  was still slightly higher than that of  $\text{CeO}_2$  NRs. The dissolved oxygen of  $\text{CeO}_2$  NRs and  $\text{CeO}_2@\text{PP}$  under the same conditions was tested as shown in Figure S1. The dissolved oxygen of bare  $\text{CeO}_2$  NRs reached 17.8 mg/L, while that of  $\text{CeO}_2@\text{PP}$  reached 23.5 mg/L. Dissolved oxygen is produced due to  $\text{Ce}^{4+}$  and  $\text{Ce}^{3+}$  which catalyze  $\text{H}_2\text{O}_2$  to  $\text{O}_2$ . The enhanced SOD and CAT activity of  $\text{CeO}_2@\text{PP}$  may be due to the functional PDA modification and coated PEG improved dispersibility and stability in aqueous solution.

## Excellent Anti-Oxidant Abilities of $\text{CeO}_2@\text{PP}$ in vitro

The cell viability test was first investigated on RAW 264.7 cells treated with  $\text{CeO}_2$  NRs and  $\text{CeO}_2@\text{PP}$  at different concentrations (0, 20, 40 and 80  $\mu\text{g/mL}$ ). As shown in Figure 2A, the concentration range (0–80  $\mu\text{g/mL}$ ) of  $\text{CeO}_2@\text{PP}$

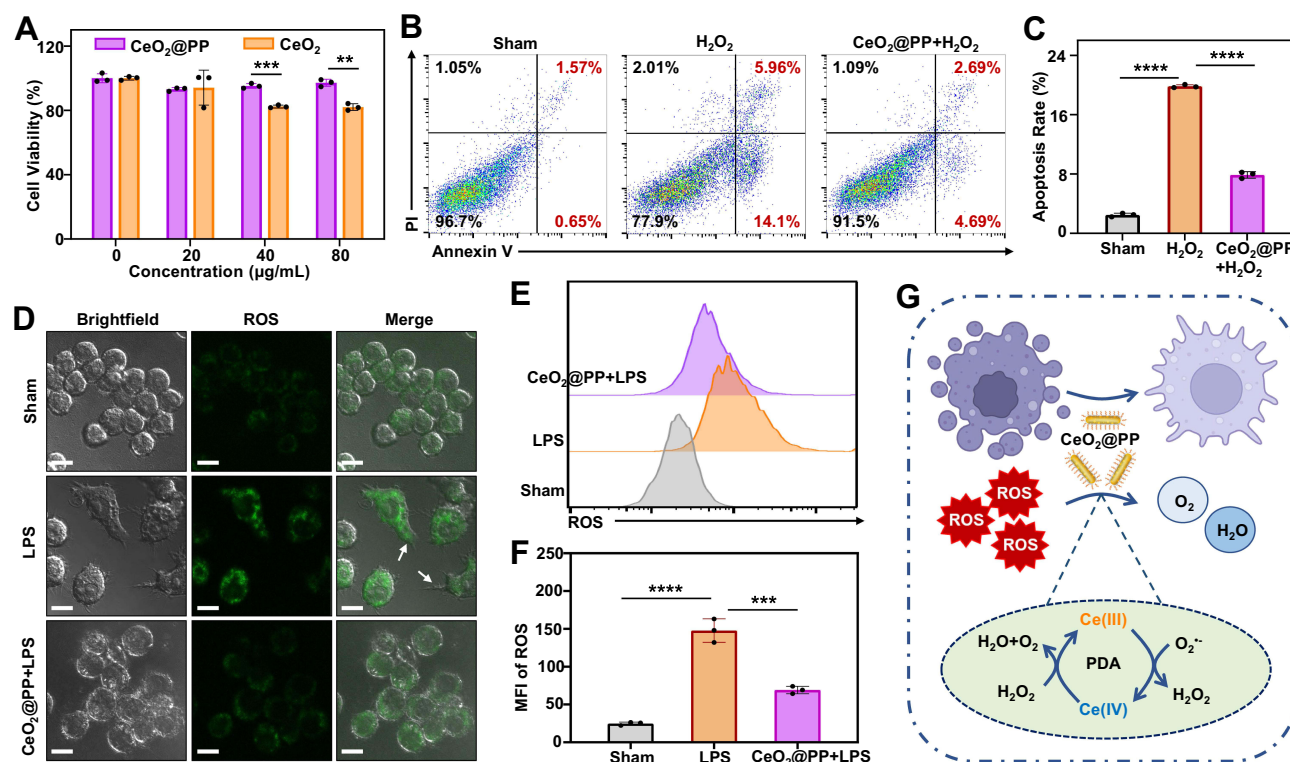


**Figure 2** ROS scavenging ability and inflammation inhibition effect of  $\text{CeO}_2@\text{PP}$ . (A) Cellular viability of RAW 264.7 macrophages incubated with different concentrations of  $\text{CeO}_2$  NRs and  $\text{CeO}_2@\text{PP}$  for 24 h. Cellular protection effects of  $\text{CeO}_2@\text{PP}$  against  $\text{H}_2\text{O}_2$ -induced apoptosis analyzed by (B) Annexin V-FITC/PI flow cytometry and (C) quantitative analysis. (D) Confocal laser scanning microscope images of intracellular ROS scavenging by  $\text{CeO}_2@\text{PP}$  in LPS-stimulated RAW 264.7 cells. Scale bar: 10  $\mu\text{m}$ , arrows indicate pseudopodia of macrophages. (E) Flow cytometry assay of intracellular ROS scavenging by  $\text{CeO}_2@\text{PP}$  in RAW 264.7 cells. (F) The mean fluorescence intensity (MFI) of ROS staining. (G) Schematic illustration of  $\text{CeO}_2@\text{PP}$  serving as a nanozyme with SOD and CAT activities to scavenge cellular ROS.  $**P < 0.01$ ;  $***P < 0.001$ ;  $****P < 0.0001$ .



had limited toxicity for RAW 264.7 cells, with cell viability greater than 95%. However, 40  $\mu\text{g/mL}$  and 80  $\mu\text{g/mL}$   $\text{CeO}_2$  showed a moderate influence on the viability of RAW 264.7 cells, which were  $82.4 \pm 0.9\%$  and  $82.0 \pm 2.1\%$ , respectively. These results confirmed that reduced toxicity was observed after PDA and PEG administration on  $\text{CeO}_2$ , indicating the excellent biocompatibility of  $\text{CeO}_2@\text{PP}$ . The cellular uptake ability of  $\text{CeO}_2@\text{PP}$ -Cy5.5 is shown in [Figure S2](#). The MFI of Cy5.5 internalized in RAW 264.7 cells was measured to be  $140.3 \pm 14.3$ ,  $144.0 \pm 5.6$  and  $136.3 \pm 2.7$  after treatment for 1 h, 3 h and 6 h, respectively, demonstrating that  $\text{CeO}_2@\text{PP}$  can be rapidly and massively internalized by RAW 264.7 cells in the early stage. Next, we used flow cytometry to investigate the protective effects of  $\text{CeO}_2@\text{PP}$  against  $\text{H}_2\text{O}_2$ -induced cell apoptosis ([Figure 2B](#)). Quantitative analysis demonstrated that the apoptotic rate of RAW 264.7 cells in the  $\text{H}_2\text{O}_2$  group was  $19.8 \pm 0.2\%$ , which was significantly increased compared with that in the sham group ( $P < 0.0001$ ). However, the apoptotic rate decreased to  $7.9 \pm 0.4\%$  with  $\text{CeO}_2@\text{PP}$  protection ([Figure 2C](#)). These data strongly indicated that  $\text{CeO}_2@\text{PP}$  could alleviate  $\text{H}_2\text{O}_2$ -mediated damage and attenuate cell apoptosis.

LPS stimulation can induce macrophages to produce large amounts of ROS. To determine the ROS scavenging ability of  $\text{CeO}_2@\text{PP}$  in the LPS-triggered inflammatory process, RAW 264.7 macrophages were treated with LPS (200 ng/mL) for 12 h. The ROS in RAW 264.7 cells were measured by CLSM ([Figure 2D](#)). The LPS group showed an effective increase in green fluorescence intensity compared with the other groups, indicating that more ROS were produced. The lower fluorescence intensity of  $\text{CeO}_2@\text{PP}$ -treated cells showed that it could reduce LPS-induced ROS in macrophages. LPS stimulation also caused an increase in macrophage size and the appearance of numerous pseudopodia, indicating that the macrophages were undergoing an immune response. The macrophages treated with  $\text{CeO}_2@\text{PP}$  did not show these morphological changes. In addition, the mean fluorescence intensity (MFI) of ROS fluorescence in each group was calculated by flow cytometry and the results are shown in [Figure 2E](#) and [F](#). The results showed that LPS significantly promoted the production of intracellular ROS, because the MFI of ROS in the LPS group was significantly higher than that in the control group.  $\text{CeO}_2@\text{PP}$  treatment significantly decreased the ROS fluorescence intensity, which directly reflected the inhibition of LPS-triggered ROS production after  $\text{CeO}_2@\text{PP}$  treatment. These data suggest that  $\text{CeO}_2@\text{PP}$  can effectively reduce intracellular ROS levels and exert a potential therapeutic effect on ROS-related cellular inflammation ([Figure 2G](#)).

## Regulating Macrophage Polarization of $\text{CeO}_2@\text{PP}$ in vitro

We next used RAW 264.7 macrophages to investigate the anti-inflammatory effect of  $\text{CeO}_2@\text{PP}$  at the cellular level ([Figure 3A](#)). As shown in [Figure 3B](#), the proportion of CD86-positive macrophages was significantly increased by the addition of LPS, and  $\text{CeO}_2@\text{PP}$  was able to reverse this change in a concentration dependent manner. In addition,  $\text{CeO}_2@\text{PP}$  increased the proportion of CD206-positive macrophages, which rises the most at a concentration of 20  $\mu\text{g/mL}$  ([Figure 3C](#)). These results indicated that  $\text{CeO}_2@\text{PP}$ , especially at a concentration of 20  $\mu\text{g/mL}$ , could effectively promote the conversion of pro-inflammatory M1-type macrophages to pro-repair M2-type macrophages. Therefore, we selected 20  $\mu\text{g/mL}$  as the subsequent treatment concentration.

We further investigated the effects of  $\text{CeO}_2@\text{PP}$  on the levels of a number of pro-inflammatory and anti-inflammatory factors using RT-qPCR. M1-type macrophage-associated pro-inflammatory mRNA levels, such as IL-1 $\beta$ , TNF- $\alpha$ , IL-6, and iNOS, were increased after LPS stimulation. As expected,  $\text{CeO}_2@\text{PP}$  treatment significantly reduced the levels of these factors ([Figure 3D](#)). Additionally, the treatment of LPS-stimulated RAW 264.7 cells with  $\text{CeO}_2@\text{PP}$  resulted in a significant reduction in the level of the proinflammatory cytokine IL-6, as determined by ELISA ([Figure S3](#)). We also examined the mRNA levels associated with M2-type macrophages, such as Arg-1 and IL-10, which are involved in anti-inflammation and tissue repair ([Figure 3E](#)). The addition of  $\text{CeO}_2@\text{PP}$  greatly promoted Arg-1 and IL-10 gene expression. Taken together, these results indicate that  $\text{CeO}_2@\text{PP}$  inhibits the expression of proinflammatory biomarkers and promotes the release of anti-inflammatory mediators, exhibiting the potential of an excellent anti-inflammatory material.

## Biodistribution and Biocompatibility Evaluation of $\text{CeO}_2@\text{PP}$ in vivo

To examine the accumulation of  $\text{CeO}_2@\text{PP}$  in colon tissue, mice were either untreated in the healthy group or challenged with 3% DSS for 7 days in the DSS group and then intraperitoneally injected with  $\text{CeO}_2@\text{PP}$ -Cy5.5 for fluorescence

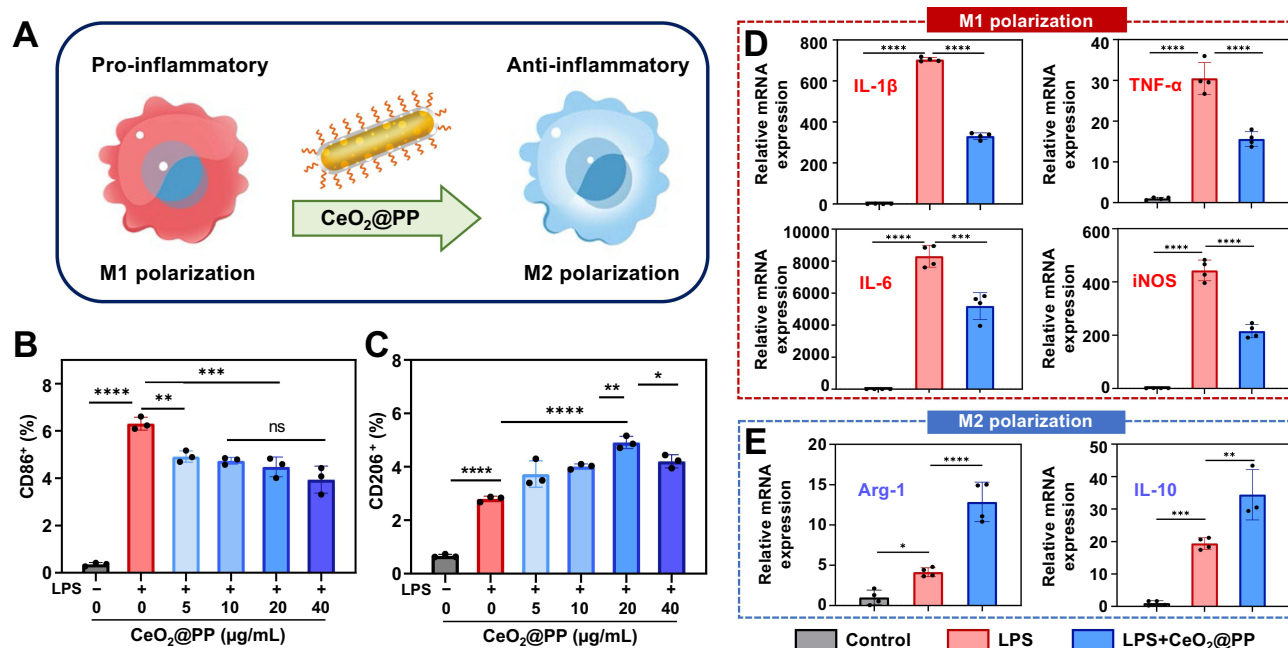


**Figure 3** Anti-inflammatory effect of CeO<sub>2</sub>@PP. (A) Schematic illustration of CeO<sub>2</sub>@PP regulating macrophage polarization. Flow cytometry quantification of (B) CD86-positive and (C) CD206-positive cells with different concentrations of CeO<sub>2</sub>@PP. (D and E) In vitro mRNA expression of pro-inflammatory biomarkers (IL-1β, TNF-α, IL-6, and iNOS) and anti-inflammatory biomarkers (Arg-1 and IL-10) with CeO<sub>2</sub>@PP (20 μg/mL) treatment against the LPS stimulation. \**p* < 0.05; \*\**p* < 0.01; \*\*\**p* < 0.001; \*\*\*\**p* < 0.0001; ns, not significant.

assessment. As shown in Figure 4A, the radiant efficiency of Cy5.5 was higher in the DSS group than in the healthy group, and enhanced accumulation and retention of CeO<sub>2</sub>@PP-Cy5.5 could be observed in the abdominal cavity except at other positions. As shown in Figure 4B, the fluorescence intensity of the colon was much stronger than that of other organs, including the heart, liver, spleen, lung, and kidney, indicating the greatest colonic retention of CeO<sub>2</sub>@PP after intraperitoneal injection. Furthermore, the radiant efficiency in the inflamed colon at 12 h after intraperitoneal injection was obviously stronger than that in the healthy colon. CeO<sub>2</sub>@PP exhibited significantly greater accumulation in the inflamed colon of colitis mice than in the colon of healthy mice at 12 h, which was consistent with 1 h and 3 h, although without a statistical difference (Figure 4C).

At present, biocompatibility is an important factor affecting the wide application of biomaterials. We further systematically investigated the potential toxicity of CeO<sub>2</sub>@PP. In terms of hemolytic capacity, ISO 10993-4 stipulates that safe biomaterials need to have a hemolysis rate less than 5%. The hemolysis rate was less than 5% after treatment with CeO<sub>2</sub>@PP (5–40 μg/mL), indicating that the hemocompatibility of CeO<sub>2</sub>@PP was satisfactory (Figure 4D). To investigate whether CeO<sub>2</sub>@PP is also biocompatible in vivo, we intraperitoneally injected CeO<sub>2</sub>@PP into healthy mice and then detected changes in major organs and blood. H&E staining did not reveal residual nanoparticles in the liver, spleen, heart, kidney or lung (Figure 4E). Compared with the PBS-treated group, no observable tissue necrosis was observed in the CeO<sub>2</sub>@PP-treated group. In addition, as shown in Figure 4F, routine blood indexes such as WBC and RBC, and blood biochemical indexes, such as ALT and AST, showed no statistically significant differences between the two groups.

## The Therapeutic Effect of CeO<sub>2</sub>@PP on Colitis in vivo

As shown in Figure 5A, we investigated whether CeO<sub>2</sub>@PP had anti-inflammatory and therapeutic effects in mice with the acute colitis model, which was built by the DSS-induced method. The mice were randomly divided into 3 groups according to the administered treatment: (1) water + PBS *i.p.*, (2) 3% DSS + PBS *i.p.* and (3) 3% DSS + CeO<sub>2</sub>@PP *i.p.* At the end of the experiment, the weight of mice in group 2 was only 73.6 ± 5.6% of the initial weight (Figure 5B), and they appeared severe diarrhea, bloody stool, drowsiness and other symptoms, which indicated that we had successfully

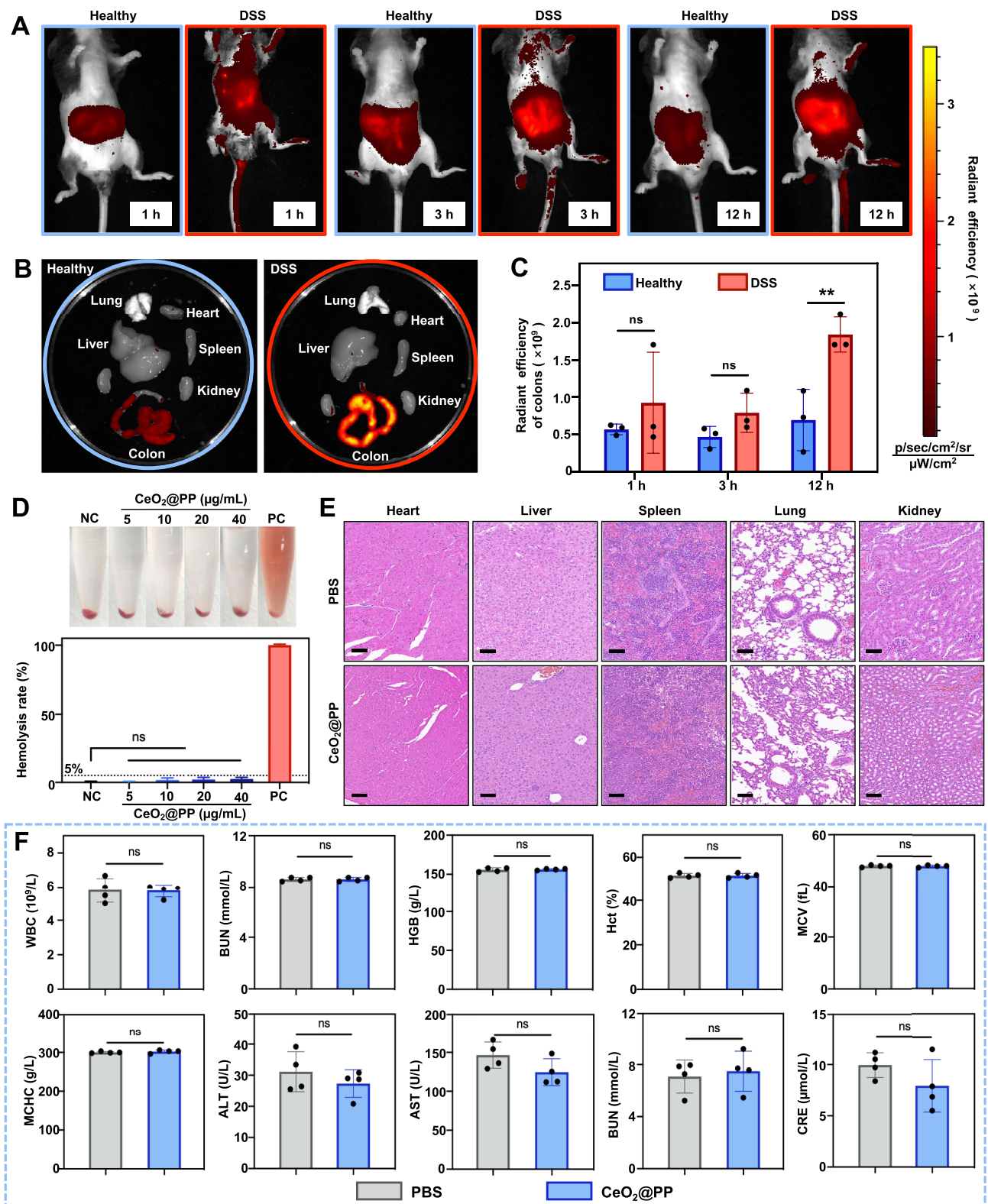


**Figure 4** Biocompatibility evaluation of  $\text{CeO}_2@\text{PP}$  in vivo. (A) Radiant efficiency of Cy5.5 in healthy and DSS-challenged mice at different timepoints. (B) Ex vivo fluorescence images of Cy5.5 in major organs of healthy and DSS-challenged mice at 12 h after intraperitoneal injection of  $\text{CeO}_2@\text{PP}$ -Cy5.5. (C) Radiant efficiency of Cy5.5 in colons from healthy and DSS-challenged mice at different timepoints. (D) Hematological indicators; (E) H&E staining images of the heart, liver, spleen, lung and kidney tissue from the mice with different treatments; scale bar: 100  $\mu\text{m}$ . (F) Blood standard hematological markers and biochemistry markers. \*\* $p < 0.01$ ; ns, not significant.

**Abbreviations:** NC, negative control; PC, positive control.



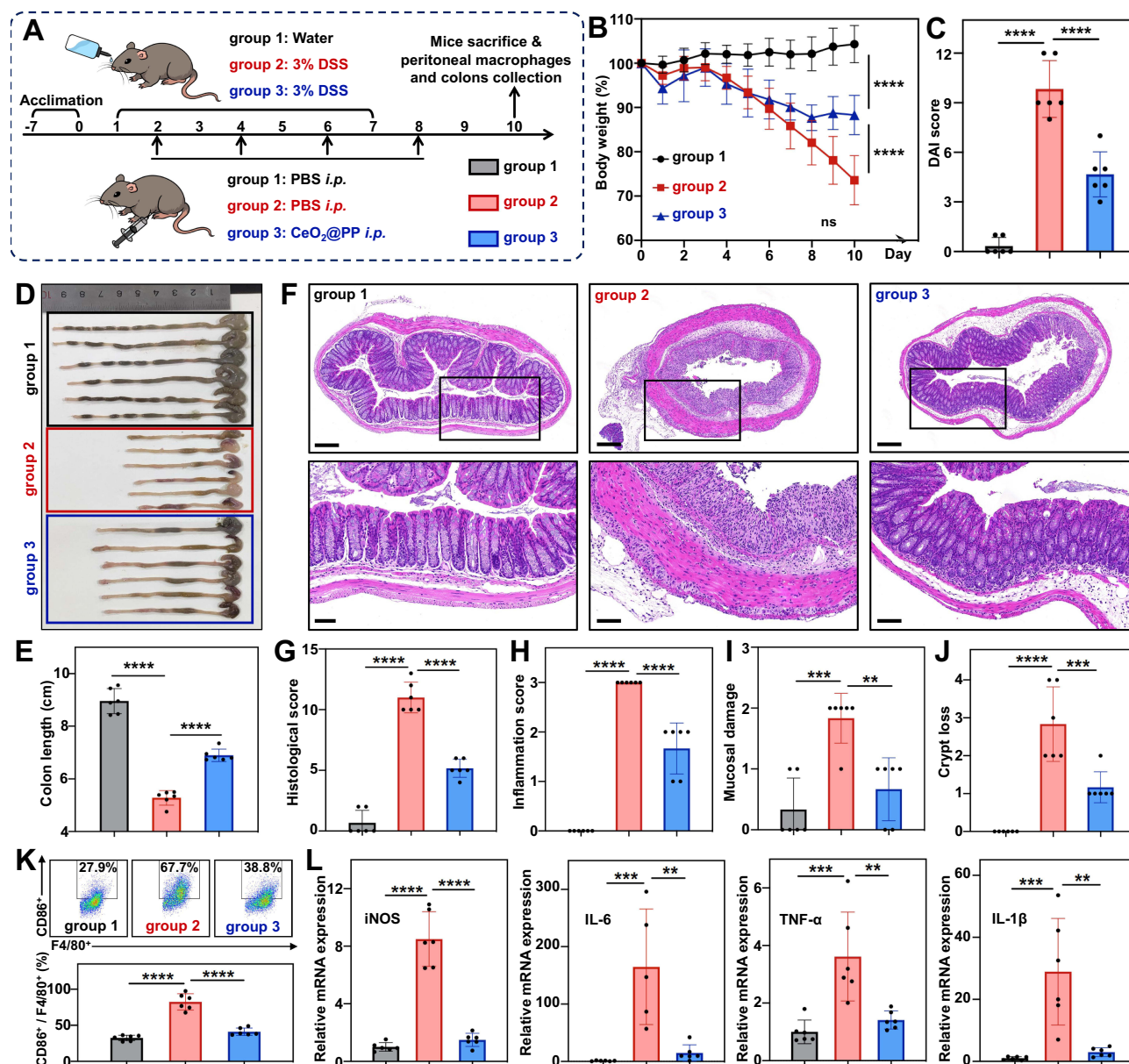


**Figure 5** The therapeutic effect of CeO<sub>2</sub>@PP on DSS-induced colitis in mice. (A) Schematic illustration of the murine colitis model and experimental protocol. C57BL/6 mice were provided H<sub>2</sub>O or DSS aqueous solution (3 wt%) drinking for 7 days, and CeO<sub>2</sub>@PP (20 μg/day) or PBS was injected intraperitoneally. (B) The weight of the mice in the control, modeling and CeO<sub>2</sub>@PP treatment groups (n = 6/group). (C) DAI scores of the mice in different groups. (D) Images of the colons and (E) the corresponding colon lengths of different groups. (F) Representative H&E-stained distal colon sections from all groups. (G) Estimation of histological colon score, including (H) inflammation severity, (I) mucosal damage and (J) crypt loss. (K) Flow cytometry analysis of the specific M1 macrophage marker CD86 in mouse peritoneal macrophages and quantification. (L) RT-qPCR analysis of iNOS, IL-6, TNF-α and IL-1β mRNA expression in distal colitis tissue. \*\**P* < 0.01; \*\*\**P* < 0.001; \*\*\*\**P* < 0.0001.

established the colitis model. The mice in group 3 were much heavier than those in group 2, although weight loss occurred. The DAI score was used to assess the overall degree of colitis in mice, which was based on weight loss, bloody stools and stool consistency. As shown in Figure 5C, the DAI of CeO<sub>2</sub>@PP-treated mice was significantly lower than that of modeling mice, quantitatively demonstrating that CeO<sub>2</sub>@PP provided symptomatic relief of colitis symptoms. When acute colitis occurs, the intestinal mucosa is damaged and the lamina propria is significantly thickened, resulting in a sharp reduction in the length of the colon. Therefore, colon length can be used to reflect the severity of colitis. Compared with the modeling group, the CeO<sub>2</sub>@PP treatment group showed significant recovery of colon length and increased solid feces in the colon, indicating that CeO<sub>2</sub>@PP has a significant therapeutic effect on DSS-induced colitis (Figure 5D and E).



As shown in Figure 5F, the H&E results showed that the colonic mucosa structure of mice in group 1 was regular. There was no obvious leukocyte infiltration in the mucosa, and clear goblet cells were regularly arranged within the lining of each crypt. In group 2, the mucosal structure of the colon was severely damaged, goblet cells were lost, a large number of inflammatory cells appeared, and the intestinal wall was also thickened. Encouragingly, histological inflammation in the colon was significantly reduced in group 3. Figure 5G shows the quantitative H&E histopathological evaluation of all groups, including the inflammation score, mucosal damage score and crypt loss score (Figure 5H–J). The scores of each item in group 3 decreased by more than half compared with group 2, which indicated the significant protective and restorative capacity of CeO<sub>2</sub>@PP for inflammatory tissues.

Immunohistochemistry of colon tissue showed that DSS treatment not only destroyed the colonic microstructure but also increased the level of IL-6 cytokine, while CeO<sub>2</sub>@PP treatment significantly decreased IL-6 production (Figure S4). Furthermore, ROS staining of colon tissue indicated that the colon tissue in group 2 showed high levels of ROS, while the colon tissue in group 3 showed low levels of ROS. Thus, these findings revealed that the intraperitoneal injection of CeO<sub>2</sub>@PP, which scavenged ROS, may be effective in the treatment of colitis (Figure S5).

Macrophages participate in the maintenance of intestinal mucosal homeostasis by differentiating into progeny with different functions. We further analyzed the mechanism of CeO<sub>2</sub>@PP treatment in colitis by measuring the polarization of macrophages in collected peritoneal lavage fluid (Figure 5K). The statistical analysis of CD86 positive cells in different groups revealed that treatment with CeO<sub>2</sub>@PP reduced the ratio of CD86<sup>+</sup> cells in F4/80<sup>+</sup> cells (M1 macrophages) from 82.5 ± 11.3% in the modeling group to 41.0 ± 5.2% in the treatment group.

Further investigation of the effects of CeO<sub>2</sub>@PP on inflammation-related biomarkers in colon tissue by RT-qPCR can provide a better understanding of the molecular mechanism of CeO<sub>2</sub>@PP in the treatment of IBD. As shown in Figure 5L, injection of CeO<sub>2</sub>@PP significantly reduced the levels of local pro-inflammatory mRNA, such as IL-6, TNF- $\alpha$  and IL-1 $\beta$ . In addition, the level of the typical proapoptotic factor iNOS, which is negatively correlated with anti-inflammatory effects, was markedly decreased after CeO<sub>2</sub>@PP treatment.

## Discussion

Although the mortality of IBD is reported to be low, long-term pathological stimulation in the intestinal mucosa will greatly increase the incidence of colon cancer in patients.<sup>36</sup> Therefore, it is of great clinical significance to develop a safe drug that can effectively treat IBD. In this study, we synthesized a nanoenzyme with CeO<sub>2</sub> nanorods as the main structure, which is capable of scavenging intracellular ROS and inhibiting the inflammatory response of macrophages. These capabilities ensured the effective application of CeO<sub>2</sub>@PP to attenuate DSS-induced acute colitis in mice.

CeO<sub>2</sub> nanoparticles exhibit antioxidant activities such as SOD and CAT properties due to the coexistence and interconversion of two oxidative states of cerium ions (Ce<sup>3+</sup> and Ce<sup>4+</sup>) on their surface.<sup>17</sup> Our results showed that CeO<sub>2</sub> can scavenge O<sub>2</sub><sup>•−</sup> and H<sub>2</sub>O<sub>2</sub> to some extent in vitro. Unfortunately, CeO<sub>2</sub> suffered from poor colloidal stability and was extremely prone to aggregation, which can be observed by DLS assay and in 24 h standing photos. It has been reported that the potential cytotoxicity of nanoparticles arises from agglomeration.<sup>37</sup> As expected, RAW 264.7 cells exhibited impaired cell viability after treatment with high concentrations of CeO<sub>2</sub>. It is well known that nanoparticles have a high tendency for adhesion and aggregation, while cerium oxide nanoparticles irreversibly aggregate after interaction with the cell culture medium.<sup>38</sup> The thinner coating modification can improve the stability of CeO<sub>2</sub> nanoparticles while maintaining their catalytic activity.<sup>39</sup> Zhang et al modified CeO<sub>2</sub> nanozymes with ultra-small citric acid and used it as an antioxidant to remove excessive ROS. This approach was successfully used to alleviate acute kidney injury caused by rhabdomyolysis.<sup>40</sup> He et al successfully enhanced the catalytic and antioxidant activities of CeO<sub>2</sub> by using in situ coating with a bioactive zeolitic imidazolate framework-8 and ultimately achieved satisfactory anti-stroke treatment efficacy.<sup>41</sup> PDA is often used as an adhesive for biomaterials due to its excellent bonding and adhesion properties.<sup>42</sup> In addition, studies have found that PDA could be enriched in inflammatory intestinal tissue and play an immunomodulatory role in reducing the inflammatory response.<sup>43,44</sup> Inspired by these researchers, we adopted a simple method to homogeneously add biocompatible coatings of PDA and PEG on the CeO<sub>2</sub> nanorod surface to overcome the above-mentioned disadvantages. The excellent adhesive property of PDA helps it adhere to CeO<sub>2</sub>, while the amine groups in the molecular structure of PDA enable further modification with hydrophilic PEG. Elemental mapping images

and FT-IR of CeO<sub>2</sub>@PP confirmed the successful coating of PDA and PEG. Because of the steric hindrance effect of polymers, their modification was able to improve the dispersion and stability of metal oxides, such as CeO<sub>2</sub>.<sup>45</sup> To our satisfaction, CeO<sub>2</sub>@PP exhibited better SOD and CAT-like catalytic activity as well as superior biocompatibility and biosafety to RAW 264.7 cells than bare CeO<sub>2</sub>.

To evaluate whether the modification of CeO<sub>2</sub> with PDA and PEG will affect the anti-oxidant ability, we assessed the intracellular ROS scavenging ability of CeO<sub>2</sub>@PP. As shown by MFI quantitative detection and CLSM observation, CeO<sub>2</sub>@PP effectively protected RAW 264.7 cells against the ROS damage induced by LPS *in vitro*. On the one hand, RAW 264.7 cells may internalize CeO<sub>2</sub>@PP through endocytic pathways. CeO<sub>2</sub> could play the role of antioxidant in multiple cell compartments, such as mitochondria, lysosomes, and endoplasmic reticulum.<sup>46</sup> On the other hand, PDA itself can be applied as an efficient scavenger for ROS. Therefore, CeO<sub>2</sub>@PP can act as an intracellular ROS scavenger in macrophages.

LPS-induced increases in endogenous ROS levels can lead to inflammatory responses in macrophages and changes in the expression of biomarkers. Both CeO<sub>2</sub> and PDA consisting of CeO<sub>2</sub>@PP were reported to effectively attenuate LPS-induced inflammatory responses.<sup>47</sup> The flow cytometry results showed that CeO<sub>2</sub>@PP treatment promoted the polarization of M2 macrophages and inhibited the polarization of M1 macrophages. In addition, CeO<sub>2</sub>@PP nanorods significantly suppressed the expression of pro-inflammatory mediators such as iNOS and IL-1 $\beta$ , and promoted the expression of anti-inflammatory biomarkers such as Arg-1 in macrophages. Most importantly, iNOS, as an M1-specific marker, is the key proinflammatory cytokine of the NF- $\kappa$ B signaling cascade.<sup>48</sup> Therefore, the anti-inflammatory ability of CeO<sub>2</sub>@PP was presumably related to the pathway regulating macrophage M2 polarization.

To further explore the clinical potential of multifunctional CeO<sub>2</sub>@PP, we detected its protective effect against ROS damage using a DSS-induced mouse colitis model. DSS disrupts the intestinal epithelium and then produces excessive ROS, which induce endogenous inflammation.<sup>49</sup> In this study, CeO<sub>2</sub>@PP was intraperitoneally injected to treat colitis because of the destruction of epithelial cells and extracellular matrix as well as the disorder of the tight epithelial barrier in colitis.<sup>50</sup> In addition, the inflamed colonic epithelium has many positively charged proteins that promote the accumulation of negatively charged nanoparticles on its surface through electrostatic interactions.<sup>51</sup> Therefore, negatively charged CeO<sub>2</sub>@PP can enter the colon through the damaged epithelium and accumulate on the inflamed epithelial surface to play a therapeutic role. CeO<sub>2</sub>@PP treatment was found to have a significant remission effect on the lesions in mouse colons, including lower DAI scores, less weight loss, milder symptoms and more slight pathological changes. In DSS-induced colitis, the proportion of M1 type peritoneal macrophages and the expression of inflammatory biomarkers increased in colon tissue.<sup>52</sup> Our results showed that CeO<sub>2</sub>@PP not only importantly reduced the proportion of M1 type peritoneal macrophages, but also greatly reduced the levels of pro-inflammatory factors in colon tissue. All these results indicate that CeO<sub>2</sub>@PP is able to exhibit powerful protective effects on tissues destroyed by inflammation.

## Conclusion

In conclusion, by coating PDA onto CeO<sub>2</sub> nanorods and attaching PEG, we have successfully prepared a novel nanozyme that can improve the colloidal stability of CeO<sub>2</sub> while retaining its high SOD and CAT activity. CeO<sub>2</sub>@PP had excellent biocompatibility, superior scavenging effects on intracellular ROS and anti-inflammatory properties on cells *in vitro*. Correspondingly, injection of CeO<sub>2</sub>@PP into mice was able to alleviate colonic inflammation without significant side effects. These results illustrated that CeO<sub>2</sub>@PP can be used as an excellent anti-inflammatory nanoplatform for IBD-like diseases.

## Acknowledgments

The authors want to appreciate AJE for professional English language editing, and BioRender for providing drawing elements, which helped visualize our research. Graphical abstract is created with BioRender.com.

## Funding

This work was funded by the National Natural Sciences Foundation of China (81571800), Jiangsu Provincial Key Research and Development Program (BE2020629), Development of Science and Technology of Nanjing (YKK19094), and “3456” Cultivation Program for Junior Talents of Nanjing Stomatological Hospital, Medical School of Nanjing University (0222R212).

## Disclosure

The authors declare no conflicts of interest in this work.

## References

- Alatab S, Sepanlou SG, Ikuta K; GBD 2017 Inflammatory Bowel Disease Collaborators. The global, regional, and national burden of inflammatory bowel disease in 195 countries and territories, 1990–2017: a systematic analysis for the global burden of disease study 2017. *Lancet Gastroenterol Hepatol*. 2020;5(1):17–30. doi:10.1016/S2468-1253(19)30333-4
- Ng SC, Shi HY, Hamidi N, et al. Worldwide incidence and prevalence of inflammatory bowel disease in the 21st century: a systematic review of population-based studies. *Lancet*. 2017;390(10114):2769–2778. doi:10.1016/S0140-6736(17)32448-0
- Park SH. Update on the epidemiology of inflammatory bowel disease in Asia: where are we now? *Intest Res*. 2022;20(2):159–164. doi:10.5217/ir.2021.00115
- Hwang J, Jin J, Jeon S, et al. SOD1 suppresses pro-inflammatory immune responses by protecting against oxidative stress in colitis. *Redox Biol*. 2020;37:101760. doi:10.1016/j.redox.2020.101760
- Tian T, Wang Z, Zhang J. Pathomechanisms of oxidative stress in inflammatory bowel disease and potential antioxidant therapies. *Oxid Med Cell Longev*. 2017;2017:1–18. doi:10.1155/2017/4535194
- Wan Y, Yang L, Jiang S, Qian D, Duan J. Excessive apoptosis in ulcerative colitis: crosstalk between apoptosis, ROS, ER stress, and intestinal homeostasis. *Inflamm Bowel Dis*. 2022;28(4):639–648. doi:10.1093/ibd/izab277
- Ban Q, Liu M, Ding N, et al. Nutraceuticals for the Treatment of IBD: current progress and future directions. *Front Nutr*. 2022;9:794169. doi:10.3389/fnut.2022.794169
- Rashed R, Valcheva R, Dieleman LA. Manipulation of gut microbiota as a key target for crohn's disease. *Front Med*. 2022;9:887044. doi:10.3389/fmed.2022.887044
- M'Koma AE. Inflammatory bowel disease: clinical diagnosis and surgical treatment-overview. *Medicina*. 2022;58(5):567. doi:10.3390/medicina58050567
- Moura FA, de Andrade KQ, Dos Santos JCF, Araújo ORP, Goulart MOF. Antioxidant therapy for treatment of inflammatory bowel disease: does it work? *Redox Biol*. 2015;6:617–639. doi:10.1016/j.redox.2015.10.006
- Dziąbowska-Grabias K, Sztanke M, Zając P, et al. Antioxidant therapy in inflammatory bowel diseases. *Antioxidants*. 2021;10(3):412. doi:10.3390/antiox10030412
- Zhao H, Zhang R, Yan X, Fan K. Superoxide dismutase nanozymes: an emerging star for anti-oxidation. *J Mater Chem B*. 2021;9(35):6939–6957. doi:10.1039/d1tb00720c
- Glorieux C, Calderon PB. Catalase, a remarkable enzyme: targeting the oldest antioxidant enzyme to find a new cancer treatment approach. *Biol Chem*. 2017;398(10):1095–1108. doi:10.1515/hsz-2017-0131
- Datta S, Rajnish KN, George Priya Doss C, Melvin Samuel S, Selvarajan E, Zayed H. Enzyme therapy: a forerunner in catalyzing a healthy society? *Expert Opin Biol Ther*. 2020;20(10):1151–1174. doi:10.1080/14712598.2020.1787980
- Wang Q, Jiang J, Gao L. Nanozyme-based medicine for enzymatic therapy: progress and challenges. *Biomed Mater*. 2021;16(4):042002. doi:10.1088/1748-605X/abe7b4
- Cheng F, Wang S, Zheng H, et al. Ceria nanoenzyme-based hydrogel with antiglycative and antioxidative performance for infected diabetic wound healing. *Small Methods*. 2022;6(11):2200949. doi:10.1002/smt.202200949
- Wu Y, Ta HT. Different approaches to synthesising cerium oxide nanoparticles and their corresponding physical characteristics, and ROS scavenging and anti-inflammatory capabilities. *J Mater Chem B*. 2021;9(36):7291–7301. doi:10.1039/D1TB01091C
- Wang M, He H, Liu D, Ma M, Zhang Y. Preparation, characterization and multiple biological properties of peptide-modified cerium oxide nanoparticles. *Biomolecules*. 2022;12(9):1277. doi:10.3390/biom12091277
- Caputo F, Mameli M, Sienkiewicz A, et al. A novel synthetic approach of cerium oxide nanoparticles with improved biomedical activity. *Sci Rep*. 2017;7(1):4636. doi:10.1038/s41598-017-04098-6
- Meng Z, Fu B, Yang Z, et al. Polydopamine-coated thalidomide nanocrystals promote DSS-induced murine colitis recovery through Macrophage M2 polarization together with the synergistic anti-inflammatory and anti-angiogenic effects. *Int J Pharm*. 2023;630:122376. doi:10.1016/j.ijpharm.2022.122376
- Liu Y, Ai K, Lu L. Polydopamine and its derivative materials: synthesis and promising applications in energy, environmental, and biomedical fields. *Chem Rev*. 2014;114(9):5057–5115. doi:10.1021/cr400407a
- Liu X, Chen W, Shao B, et al. Mussel patterned with 4D biodegrading elastomer durably recruits regenerative macrophages to promote regeneration of craniofacial bone. *Biomaterials*. 2021;276:120998. doi:10.1016/j.biomaterials.2021.120998
- Cheng W, Nie J, Xu L, et al. pH-Sensitive delivery vehicle based on folic acid-conjugated polydopamine-modified mesoporous silica nanoparticles for targeted cancer therapy. *ACS Appl Mater Interfaces*. 2017;9(22):18462–18473. doi:10.1021/acsami.7b02457
- Ding X, Liu J, Li J, et al. Polydopamine coated manganese oxide nanoparticles with ultrahigh relaxivity as nanotheranostic agents for magnetic resonance imaging guided synergetic chemo-/photothermal therapy. *Chem Sci*. 2016;7(11):6695–6700. doi:10.1039/c6sc01320a
- Wei Y, Gao L, Wang L, et al. Polydopamine and peptide decorated doxorubicin-loaded mesoporous silica nanoparticles as a targeted drug delivery system for bladder cancer therapy. *Drug Deliv*. 2017;24(1):681–691. doi:10.1080/10717544.2017.1309475
- Rai N, Kanagaraj S. Enhanced antioxidant ability of PEG-Coated Ce<sub>0.5</sub>Zr<sub>0.5</sub>O<sub>2</sub>-based nanofluids for scavenging hydroxyl radicals. *ACS Omega*. 2022;7(26):22363–22376. doi:10.1021/acsomega.2c01266
- Fisher TJ, Zhou Y, Wu TS, Wang M, Soo YL, Cheung CL. Structure-activity relationship of nanostructured ceria for the catalytic generation of hydroxyl radicals. *Nanoscale*. 2019;11(10):4552–4561. doi:10.1039/c8nr09393h
- Zhang Y, Wu X, Hou C, et al. Dual-responsive dithio-polydopamine coated porous CeO<sub>2</sub> nanorods for targeted and synergistic drug delivery. *IJN*. 2018;13:2161–2173. doi:10.2147/IJN.S152002
- Meng F, Sun Y, Lee RJ, et al. Folate receptor-targeted albumin nanoparticles based on microfluidic technology to deliver cabazitaxel. *Cancers*. 2019;11(10):1571. doi:10.3390/cancers11101571

30. Liu YJ, Tang B, Wang FC, et al. Parthenolide ameliorates colon inflammation through regulating Treg/Th17 balance in a gut microbiota-dependent manner. *Theranostics*. 2020;10(12):5225–5241. doi:10.7150/thno.43716
31. Abdallah HMI, Ammar NM, Abdelhameed MF, et al. Protective mechanism of acacia saligna butanol extract and its nano-formulations against ulcerative colitis in rats as revealed via biochemical and metabolomic assays. *Biology*. 2020;9(8):195. doi:10.3390/biology9080195
32. Binabaj MM, Asgharzadeh F, Avan A, et al. EW-7197 prevents ulcerative colitis-associated fibrosis and inflammation. *J Cell Physiol*. 2019;234(7):11654–11661. doi:10.1002/jcp.27823
33. Qu J, Chen D, Li N, et al. 3D gold-modified cerium and cobalt oxide catalyst on a graphene aerogel for highly efficient catalytic formaldehyde oxidation. *Small*. 2018;1804415. doi:10.1002/sml.201804415
34. He Y, Wang J, Zhang H, et al. Polydopamine-modified graphene oxide nanocomposite membrane for proton exchange membrane fuel cell under anhydrous conditions. *J Mater Chem A*. 2014;2(25):9548. doi:10.1039/c3ta15301k
35. Yuan Qiang Z, Zhao Li J, Liu Y, et al. Systemic delivery of micelles loading with paclitaxel using N-succinyl-palmitoyl-chitosan decorated with cRGDyK peptide to inhibit non-small-cell lung cancer. *Int J Pharm*. 2015;492(1–2):141–151. doi:10.1016/j.ijpharm.2015.07.022
36. Shah SC, Itzkowitz SH. Colorectal cancer in inflammatory bowel disease: mechanisms and management. *Gastroenterology*. 2022;162(3):715–730. e3. doi:10.1053/j.gastro.2021.10.035
37. Gupta A, Das S, Neal CJ, Seal S. Controlling the surface chemistry of cerium oxide nanoparticles for biological applications. *J Mater Chem B*. 2016;4(19):3195–3202. doi:10.1039/c6tb00396f
38. Mekaru H. Effect of agitation method on the nanosized degradation of polystyrene microplastics dispersed in water. *ACS Omega*. 2020;5(7):3218–3227. doi:10.1021/acsomega.9b03278
39. Lee SS, Song W, Cho M, et al. Antioxidant properties of cerium oxide nanocrystals as a function of nanocrystal diameter and surface coating. *ACS Nano*. 2013;7(11):9693–9703. doi:10.1021/nn4026806
40. Zhang DY, Liu H, Li C, et al. Ceria nanozymes with preferential renal uptake for acute kidney injury alleviation. *ACS Appl Mater Interfaces*. 2020;12(51):56830–56838. doi:10.1021/acsami.0c17579
41. He L, Huang G, Liu H, Sang C, Liu X, Chen T. Highly bioactive zeolitic imidazolate framework-8-capped nanotherapeutics for efficient reversal of reperfusion-induced injury in ischemic stroke. *Sci Adv*. 2020;6(12):eaay9751. doi:10.1126/sciadv.aay9751
42. Li J, Xia Q, Guo H, et al. Decorating bacteria with triple immune nanoactivators generates tumor-resident living immunotherapeutics. *Angew Chem Int Ed*. 2022;61(27):e202202409. doi:10.1002/anie.202202409
43. Pan C, Li J, Hou W, et al. Polymerization-mediated multifunctionalization of living cells for enhanced cell-based therapy. *Adv Mater*. 2021;33(13):2007379. doi:10.1002/adma.202007379
44. Li J, Hou W, Lin S, et al. Polydopamine nanoparticle-mediated dopaminergic immunoregulation in colitis. *Advanced Science*. 2022;9(1):2104006. doi:10.1002/advs.202104006
45. Jin A, Wang Y, Lin K, Jiang L. Nanoparticles modified by polydopamine: working as “drug” carriers. *Bioact Mater*. 2020;5(3):522–541. doi:10.1016/j.bioactmat.2020.04.003
46. Rubio L, Annangi B, Vila L, Hernández A, Marcos R. Antioxidant and anti-genotoxic properties of cerium oxide nanoparticles in a pulmonary-like cell system. *Arch Toxicol*. 2016;90(2):269–278. doi:10.1007/s00204-015-1468-y
47. Wang Y, Li C, Wan Y, et al. Quercetin-loaded ceria nanocomposite potentiate dual-directional immunoregulation via macrophage polarization against periodontal inflammation. *Small*. 2021;14:2101505.
48. Cinelli MA, Do HT, Miley GP, Silverman RB. Inducible nitric oxide synthase: regulation, structure, and inhibition. *Med Res Rev*. 2020;40(1):158–189. doi:10.1002/med.21599
49. Eichele DD, Kharbanda KK. Dextran sodium sulfate colitis murine model: an indispensable tool for advancing our understanding of inflammatory bowel diseases pathogenesis. *World J Gastroenterol*. 2017;23(33):6016–6029. doi:10.3748/wjg.v23.i33.6016
50. Zhang Q, Tao H, Lin Y, et al. A superoxide dismutase/catalase mimetic nanomedicine for targeted therapy of inflammatory bowel disease. *Biomaterials*. 2016;105:206–221. doi:10.1016/j.biomaterials.2016.08.010
51. Lee Y, Sugihara K, Gilliland MG, Jon S, Kamada N, Moon JJ. Hyaluronic acid–bilirubin nanomedicine for targeted modulation of dysregulated intestinal barrier, microbiome and immune responses in colitis. *Nat Mater*. 2020;19(1):118–126. doi:10.1038/s41563-019-0462-9
52. Cao X, Duan L, Hou H, et al. IGF-1C hydrogel improves the therapeutic effects of MSCs on colitis in mice through PGE<sub>2</sub>-mediated M2 macrophage polarization. *Theranostics*. 2020;10(17):7697–7709. doi:10.7150/thno.45434

## International Journal of Nanomedicine

Dovepress

## Publish your work in this journal

The International Journal of Nanomedicine is an international, peer-reviewed journal focusing on the application of nanotechnology in diagnostics, therapeutics, and drug delivery systems throughout the biomedical field. This journal is indexed on PubMed Central, MedLine, CAS, SciSearch®, Current Contents®/Clinical Medicine, Journal Citation Reports/Science Edition, EMBASE, Scopus and the Elsevier Bibliographic databases. The manuscript management system is completely online and includes a very quick and fair peer-review system, which is all easy to use. Visit <http://www.dovepress.com/testimonials.php> to read real quotes from published authors.

Submit your manuscript here: <https://www.dovepress.com/international-journal-of-nanomedicine-journal>